
Article:
Abdoulla-Latiwish, KOA, Mao, X and Jaworski, AJ (2017) Thermoacoustic micro-electricity generator for rural dwellings in developing countries driven by waste heat from cooking activities. Energy, 134. pp. 1107-1120. ISSN 0360-5442

https://doi.org/10.1016/j.energy.2017.05.029

Accepted Manuscript

Thermoacoustic micro-electricity generator for rural dwellings in developing countries driven by waste heat from cooking activities

Kalid O.A. Abdoulla-Latiwish, Xiaoan Mao, Artur J. Jaworski

PII:	S0360-5442(17)30785-5
DOI:	10.1016/j.energy.2017.05.029
Reference:	EGY 10836
To appear in:	*Energy*
Received Date:	10 January 2017
Revised Date:	03 May 2017
Accepted Date:	05 May 2017

Please cite this article as: Kalid O.A. Abdoulla-Latiwish, Xiaoan Mao, Artur J. Jaworski, Thermoacoustic micro-electricity generator for rural dwellings in developing countries driven by waste heat from cooking activities, *Energy* (2017), doi: 10.1016/j.energy.2017.05.029

Highlights

- Demonstrator with just under 20 W of electrical output is modelled and tested
- Design trade-offs are outlined to apply the technology in poor rural areas
- Atmospheric air has been shown as a viable thermodynamic medium
- Use of cheap components has been demonstrated to reduce costs
- Acoustic and electric efficiencies of 3.5 % and 1.9%, respectively, achieved

Thermoacoustic micro-electricity generator for rural dwellings in developing countries driven by waste heat from cooking activities

Kalid O.A. Abdoulla-Latiwish, Xiaoan Mao and Artur J. Jaworski*

Faculty of Engineering, University of Leeds
Woodhouse Lane, Leeds LS2 9JT, UK

*Corresponding author: a.j.jaworski@leeds.ac.uk

Abstract

Thermoacoustic engines convert heat into acoustic power without moving parts. Coupling them with electrodynamic transducers – directly converting acoustic power to electricity – enables building simple electricity generators, where the only moving part is the piston of the linear alternator. Integration of such devices with biomass-driven cook stoves widely used in remote and rural areas of developing countries can lead to inexpensive electrical power systems, essentially powered by waste heat from daily cooking activities. In this paper the modelling, design, construction and testing of a laboratory demonstrator of such generator is outlined. A travelling-wave thermoacoustic engine with a looped-tube configuration is modelled using DeltaEC tool and constructed to convert heat input to acoustic power. Flue gas from a propane burner is used as a heat source for demonstration purposes. An audio loudspeaker is connected to a side branch and adopted as the electro-dynamic transducer for electricity production. Atmospheric air is employed as the working fluid to keep the cost of future systems low. The demonstrator produced just under 20 W of electricity with thermal-to-acoustic and thermal-to-electric efficiencies of around 3.5% and 1.9%, respectively, which demonstrates the micro-power source concept. Experimental results and their numerical validation are outlined and analysed.

Keywords: waste heat; cooking; electricity generator; micro-power; developing countries; thermoacoustics

NOMENCLATURE

Symbols	
a	speed of sound, [$m \cdot s^{-1}$]
A	cross sectional area, [m^2]
Bl	Bl product, [$N \cdot A^{-1}$]
c	heat capacity, [$J \cdot kg^{-1} \cdot K^{-1}$]
f	frequency, [Hz] spatially averaged diffusion function, -
F	loudspeaker resonance frequency, [Hz]
$\dot{H}$	total power, [W]
i	imaginary unit, $\sqrt{-1}$
Im	imaginary value, -
k	thermal conductivity, [$W \cdot m^{-1} \cdot K^{-1}$]
K	spring stiffness, [$N \cdot m^{-1}$]
L	inductance, [H]
M	mass, [kg]
p	pressure, [Pa]
Q	thermal power, heat, [W]
R	Resistance, [Ω]
Re	real value, -
T	temperature, [K], [°C]
U	volumetric velocity, [$m^3 \cdot s^{-1}$]
$\dot{W}$	power (rate of work), [W]
x	spatial coordinate, [m]
X	maximum displacement, [m]
Z	acoustic impedance, [$Pa \cdot s \cdot m^{-3}$]
β	thermal expansion coefficient, [K^{-1}]
γ	ratio of isobaric to isochoric specific heats, -
δ	penetration depth, [m]
ε_s	correction factor for finite solid heat capacity, -
ϕ	phase angle, [rad]
ρ	density, [$kg \cdot m^{-3}$]
σ	Prandtl number, -

ω	angular frequency [s^{-1}]
~	complex conjugate, -
Subscripts	
a	Acoustic
alt	alternator
e	electrical
m	mean mechanical
p	isobaric
1	indicates complex amplitude
κ	thermal
v	viscous
Abbreviations	
ALT	Alternator
CHX	Cold Heat Exchanger
DeltaEC	Design Environment for Low-Amplitude Thermoacoustic Energy Conversion
HHX	Hot Heat Exchanger
REG	Regenerator
SCORE	**S**tove for **Co**oking **R**efrigeration and **E**lectricity Supply
S/S	Stainless steel
TBT	Thermal Buffer Tube

1. Introduction

Fundamentally, thermoacoustic effect is understood as a thermodynamic interaction between an acoustic wave and solid material, the latter having a temperature gradient imposed in the direction of the acoustic wave propagation. A qualitative explanation of the thermoacoustic effect was given over 100 years ago by Lord Rayleigh [1] as follows: "If heat be given to the air at the moment of greatest condensation, or be taken from it at the moment of greatest rarefaction, the vibration is encouraged". In essence, as the acoustic wave is imposed in a compressible fluid (gas), an individual gas "parcel" experiences a cyclic translational movement coupled with a cycle of compression and expansion processes giving rise to its temperature changes within an acoustic cycle. However, the close vicinity of a solid material also allows for the thermal energy transfer between the gas and the solid over the distance of the translational movement (referred to as acoustic displacement amplitude) within an acoustic cycle. Therefore, for the appropriately phased pressure and displacement oscillations, near a solid material with favourable thermal conditions, it is possible to subject the compressible fluid to a useful thermodynamic cycle. The description by Lord Rayleigh cited above actually refers to the case of a "thermoacoustic engine" where thermoacoustic instability is allowed to grow spontaneously – the process in effect converts heat energy into acoustic (i.e. mechanical) form of energy. Using appropriate design methods, the acoustic power production can reach levels of practical significance. Such thermoacoustic engines are an emerging technology for energy conversion, especially for energy recovery from relatively low temperature heat sources – for example waste heat with temperatures as low as 80°C. Some previous work in this area is described for example in references [2-9].

Applications and development of thermoacoustic energy conversion technologies have been reviewed in detail elsewhere (e.g. [10]) and therefore only the information pertinent to the current paper will be outlined here. This includes a specific type of thermoacoustic devices, namely a travelling wave thermoacoustic engine, which is described briefly. Figure 1a shows the so-called "core" of the engine consisting of a regenerator (essentially a piece of porous material) and a pair of (hot and cold) heat exchangers to build up a temperature gradient along the regenerator. The core acts as a power amplifier: acoustic power is fed into the thermoacoustic core at the cold heat exchanger end, and after the amplification within the regenerator, a larger amount of acoustic power flows out from the hot heat exchanger end of the thermoacoustic core. A positive feedback can be achieved by connecting the hot and cold ends of the thermoacoustic core via an acoustic wave guide (also referred to as feedback pipe, cf. later Fig. 4), and thus the acoustic oscillation can be maintained[1]. Of course not all of the acoustic power needs to be diverted back to the thermoacoustic core. Indeed, there is an excess

[1] Fig. 1 also has "resonator duct" marked. Clearly any internal components of the engine such as the "core" must be contained in an "acoustic network" formed of various pipes which serve as waveguides for the acoustic wave (or acoustic power flow). Generally such networks are called thermoacoustic resonators, but some of their parts have more specific functions and are separately named "thermal buffer tubes", "stubs", "feedback pipes" etc. which highlights their specific roles within the network (or the resonator).

of the acoustic power leaving the core that can be utilized usefully, for example by extracting electrical power, as long as there is a sufficient part of the acoustic power returning back to the cold end of the core in order to sustain the amplification process. A steep temperature gradient is maintained within the regenerator by the heat exchangers – thermodynamically speaking heat is added to the system through the hot heat exchanger ($Q_{\text{heat source}}$) and removed through the cold heat exchanger (Q_{sink}) in order to generate mechanical energy (acoustic power).

Key interactions between the oscillating gas and solid material of the regenerator can of course be looked into in some more detail. Figure 1b illustrates the physics behind the process. An acoustic travelling wave propagates through the regenerator in the direction from the cold towards the hot heat exchanger. Here, the thermal contact between the gas and solid material is very good because of the appropriate selection of the pore size, and thus the gas undergoes a Stirling-like thermodynamic cycle. The gas expands while displaced towards the higher temperature and compresses while displaced towards the lower temperature [11, 12]. This allows obtaining the correct phasing between the gas parcel displacement and its compression in order to convert thermal energy to mechanical (i.e. acoustic) power. In this sense the travelling wave thermoacoustic engine can be likened to the acoustic version of Stirling engine (as illustrated in Fig. 1c). The favourable timing for the Stirling-like cycle to take place is ensured by a compact acoustic network (not shown in Fig 1) rather than the crank and piston mechanism. It has been recently demonstrated that "top-end" high pressure travelling wave thermoacoustic heat engines can achieve a thermal efficiency (i.e. heat to acoustics) equivalent to 49% of Carnot efficiency [13]. However, despite involved thermodynamics, there are no mechanical moving parts to execute the thermodynamic cycle, which provides an opportunity for constructing high reliability and low maintenance devices. In addition, the working gas in thermoacoustic engines is typically a high pressure noble gas (typical pressures could be up to 50-60 bar) which make thermoacoustic devices environmentally benign, especially in refrigeration applications where no ozone depleting chemicals need to be used. Moreover, the temperature difference required to drive the thermodynamic cycle could be relatively small. For instance, de Blok's [9] travelling-wave engine undergoes excitation at an onset temperature difference across regenerator of only 65K. This gives the potential for the thermoacoustic technology to be utilized in conjunction with renewable energy sources (concentrated solar power, geothermal energy or sustainable biomass combustion) or waste heat sources, typically available across many process industries.

Usually, the acoustic power generated by the thermoacoustic engine can be directly converted to electricity through the electro-dynamic transduction mechanism (for example using high efficiency flexure bearing supported linear alternators). The thermoacoustic engine coupled to the linear alternator is referred to as a thermoacoustic generator, some examples described in references [14,15]. The travelling-wave thermoacoustic electricity generator developed by Backhaus et al. [14] for space

applications achieved the electrical output around 60 W, while the maximum thermal to electrical efficiency of the system was 18%. Wu et al. [15] reported a generator system capable of delivering 500 W of electricity at the thermal to electrical efficiency of 15%. However, inevitably the high performance systems tend to be very costly mainly due to the requirement for having high pressure working fluids and high efficiency alternators that may cost up to several thousands of US dollars.

The work presented in this paper is part of a broader research consortium, SCORE (Stove for Cooking Refrigeration and Electricity Supply), which aims to develop a cook stove for remote and rural communities of developing countries that should provide the function of micro-generation of electricity as well as some refrigeration capability for storage of medical supplies. There is a clear need for developing such devices since over 3.3 billion people live in rural areas, 2.4 billion use biomass for cooking and about 2 billion are without access to electricity. Clearly, a complex project of this nature needs to be subdivided into more manageable tasks. These include in particular: (1) social science studies, and in particular identification of the energy requirements of the communities concerned [16, 17]; (2) design of the stove from the point of view of low cost [18]; (iii) development of the hardware fulfilling the requirements on electricity generation and cooling (cf. [19]) sides.

It is also apparent from the social science research [16,17], already conducted by the consortium, that the electrical power rating of an ideal system for rural dwellings in developing countries should aim at peak electrical power levels between 50 and 150 W, at a price that should ideally be below 100 US dollars[2], while some communities indicated that even a modest power output of 15-20 W of electricity per dwelling could make a huge difference to everyday lives. Generating these amounts of electricity as a by-product of cooking activities (essentially biomass burning) would be therefore of immense benefit from the social perspective. Moreover, such applications are not efficiency-limited since the waste heat produced isn't otherwise utilised. The social science research estimates are based on the coking activities of approximately 4 to 6 hours per day (morning and evening meals).

This paper is devoted to the development of a technology demonstrator – namely a suitable thermoacoustic electricity generator sub-system to be integrated into the ultimate stove design. Whilst dealing with the technical challenges, the work also addresses a low-cost design philosophy, in particular utilization of atmospheric air as a working gas and easily available PVC components. However, cost and economics aspects are not a subject of rigorous analysis in this paper. This has already been a subject of consortium's research led by the charity Practical Action.

The work presented here is a next step from an early "proof-of-concept": a generator capable of producing just below 10 W of electricity, using electrical heaters to mimic thermal input, and a

[2] Numerically, this corresponds to a range between just under $700/kW to $2,000/kW, although such comparisons have limited use in situations where a few tens of watts make all the difference to a rural dwelling. Similarly, they are not scalable to kW range by multiplying costs of a 50W or a 150W device.

loudspeaker placed "in series" within the loop of a travelling wave thermoacoustic engine [20]. Current technology demonstrator is capable of producing just under 20 W of electricity using the flue gases from a propane burner to simulate biomass combustion and power the thermoacoustic engine. The acoustic network has been also significantly re-designed to incorporate a different loudspeaker model (cf. Table 1 vs. data provided in [20]) located in a "side branch" (cf. Fig. 3) rather than "in series" (as explained in [20]) in order to increase the output electrical power. Of course in what is described here, a low power and low efficiency system is discussed, due to the use of air at atmospheric pressure. In what is to follow, sections 2 and 3 deal with the issues of design principles and modelling the system using DeltaEC. Section 4 deals with the description of laboratory setup of the demonstrator. Section 5 contains the results describing the system performance, while section 6 focuses on general conclusions and outlines future work on further development of the generator.

2. Design strategy of the demonstrator

Given the socio-economic aspects explained above, the design of the demonstrator has to be different from that typically used in the conventional high pressure thermoacoustic devices, which usually aim to achieve a high power production, high power densities[3] and high energy conversion efficiencies. It needs to be explained that a high mean pressure inside the loop is preferred as the power density is proportional to the mean pressure [21]. However, any increase in the mean pressure should be taken into account with consideration of the following two issues. Firstly, any increase in the mean pressure leads to decreased thermal contact between the gas parcels and the solid in the regenerator and the hot heat exchanger. This occurs because the thermal penetration depth δ_k is inversely proportional to the mean density (and hence to the mean pressure) according the following relationship:

$$\delta_k = \sqrt{\frac{2k}{\omega \rho_m c_p}} \tag{1}$$

where k is thermal conductivity , ω is angular frequency, ρ_m is gas density and c_p is isobaric specific heat of the working gas. To combat this one would need to decrease the hydraulic radius of these components, but unfortunately this would result in high fabrication costs which would not be acceptable for the current end-user. Secondly, increasing the mean pressure also requires a high pressure vessel which increases the cost of the generator. Therefore, and due to these reasons, the mean pressure inside the generator is kept at atmospheric pressure. While thermodynamically such a design is of limited performance it becomes of practical value, namely it is possible to use very cheap pipes and fittings made of PVC as parts of acoustic network.

The choice of the travelling wave looped-tube type of the thermoacoustic engine (compared to its standing wave counterparts) is made from the point of view of maximizing the thermodynamic efficiency whilst minimizing the viscous losses which is possible in the feedback-loop waveguide when the phasing

[3] In thermoacoustic terminology "power density" refers to the amount of acoustic power carried per unit area of duct cross section.

between pressure and velocity oscillations is near 0º. These requirements result in the application of a "matching stub" and an increase in the diameter of the thermoacoustic core compared to the feedback pipe. The latter is because the acoustic impedance of the thermoacoustic core must be much larger than the acoustic impedance in the feedback pipe [8]. Therefore, the ratio of the cross sectional area of the thermoacoustic core to the cross sectional area of the feedback pipe must be much larger than 1.

The working frequency of the generator considered here must be selected after consideration of several issues. Firstly, the working frequency should be near the resonance frequency of the alternator so that only a relatively small acoustic pressure (or acoustic pressure difference) is needed to excite the alternator. Secondly, the increase in the frequency increases the power density in the loop [22], which would be desirable, but may be at the cost of a reduced acoustic to electric power conversion efficiency. Unfortunately, the thermal penetration depth δ_k decreases as the frequency increases according to Equation (1). As a result, when increasing the frequency, similar problems occur as in the already mentioned case of increasing the mean pressure: namely it becomes too cumbersome and costly to build very fine regenerator and heat exchanger structures. Therefore, the working frequency should be a trade-off between the factors mentioned above.

The ultimate target of an inexpensive design is likely to exclude the commercial linear alternators as these may cost up to several thousand US dollars. These have acoustic-to-electric efficiencies in excess of 80%. Cheap alternatives for linear alternators are audio loudspeakers or re-designed units based on conventional loudspeaker parts, for which the resonance frequencies are generally in the range of 40-80 Hz. Their acoustic-to-electric efficiencies tend to be between 40 and 55%. As already outlined, in travelling wave devices, some of the acoustic power produced in the regenerator flows into the loop and is extracted by the alternator to be converted into electric power. Inserting the alternator in the loop to stop the acoustic streaming as a second function besides the main function of producing electricity would in principle be beneficial [20]. However, this arrangement may cause unnecessary disturbance to the acoustic field where there is high pressure drop caused by the alternator [23], which subsequently limits the acoustic power in the loop. Instead, the suppression of the acoustic streaming could be achieved in principle by inserting an elastic membrane.

The heating power input into the shell-and-tube type of hot heat exchanger of the demonstrator is to show the feasibility of using heat from a real cooking stove. Therefore, the heating power absorbed from flue gas provided by a propane burner is considered in this study for the demonstration. The hydraulic radius of the tubes of the heat exchanger should be in the range of 2-5 times the thermal penetration depth δ_k in the heat exchanger. This is to ensure good thermal contact between the oscillating gas and the walls of the tubes. Of course, the use of atmospheric air leads to an easier manufacture of heat exchangers due to relaxed dimensions for welding processes.

3. DeltaEC modelling

Following the considerations outlined in section 2, it is necessary to conduct parametric studies of the system performance. This is done using a widely accepted computer simulation tool DeltaEC (Design Environment for Low-Amplitude Thermoacoustic Energy Conversion) which was developed by Los Alamos National Laboratory over the last two decades. It is capable of simulating a range of different acoustic and thermoacoustic networks made up from basic "blocks", forming the complex structures of thermoacoustic engines and refrigerators [24]. Swift [2] analysed the accuracy of DeltaEC predictions; it is generally accepted that the linear theory assumptions hold well up to drive ratio (ratio of pressure amplitude to mean pressure) of around 5%, while significant departures can be observed for drive ratios in excess of 10% (note in particular discrepancies between measured and calculated (pressure amplitude)^2 – indicative of acoustic power level – that show >30% mismatch in Figure 10 in [2]). Despite these shortcomings DeltaEC is an invaluable tool in the iterative "design-build-verify" process giving the required insight into the properties of acoustic field for further improvements.

The program utilizes the linear theory to integrate one dimensional wave equation over a geometrical segment or a number of segments that are included in a thermoacoustic device such as ducts, cones, heat exchangers, thermal buffer tubes[4], stacks and regenerators. This integration solves the coupling equations of the acoustic pressure (p_1), volumetric velocity (U_1), the mean gas temperature (T_m) and the total power ($\dot{H}_2$), over the connected segments [25]. The governing equations can be presented as follows [25]:

[4] In simple terms thermal buffer tube (TBT) separates hot and ambient heat exchangers in travelling-wave thermoacoustic engines. It passes acoustic wave while minimizing heat transport.

$$\frac{dp_1}{dx} = -\frac{i\omega\rho_m}{A(1-f_v)}U_1 , \tag{2}$$

$$\frac{dU_1}{dx} = -\frac{i\omega A}{\rho_m a^2}\left[1+\frac{(\gamma-1)f_k}{1+\varepsilon_s}\right]p_1 + \frac{\beta(f_k-f_v)}{(1-f_v)(1-\sigma)(1+\varepsilon_s)}\frac{dT_m}{dx}U_1 , \tag{3}$$

$$\frac{dT_m}{dx} = \frac{\dot{H}_2 - \frac{1}{2}\mathrm{Re}\left[p_1\tilde{U}_1\left(1-\frac{T_m\beta(f_k-\tilde{f}_v)}{(1+\varepsilon_s)(1+\sigma)(1-\tilde{f}_v)}\right)\right]}{\frac{\rho_m c_p|U_1|^2}{2A\omega(1-\sigma)|1-f_v|^2}\mathrm{Im}\left(\tilde{f}_v+\frac{(f_k-\tilde{f}_v)\left(1+\frac{\varepsilon_s f_v}{f_k}\right)}{(1+\varepsilon_s)(1+\sigma)}\right)-(Ak+A_{solid}k_{solid})} , \tag{4}$$

$$\dot{H}_2 = \frac{\rho_m c_p|U_1|^2}{2A\omega(1-\sigma)|1-f_v|^2}\frac{dT_m}{dx}\mathrm{Im}\left(\tilde{f}_v+\frac{(f_k-\tilde{f}_v)\left(1+\frac{\varepsilon_s f_v}{f_k}\right)}{(1+\varepsilon_s)(1+\sigma)}\right)-(Ak+A_{solid}k_{solid})\frac{dT_m}{dx}+$$
$$+\frac{1}{2}\mathrm{Re}\left[p_1\tilde{U}_1\left(1-\frac{T_m\beta(f_k-\tilde{f}_v)}{(1+\varepsilon_s)(1+\sigma)(1-\tilde{f}_v)}\right)\right]. \tag{5}$$

The production or dissipation of the acoustic power can be represented by [26]:

$$\frac{d\dot{W}_a}{dx} = \frac{1}{2}Re\left[\tilde{U}_1\frac{dp_1}{dx}+\tilde{p}_1\frac{dU_1}{dx}\right] . \tag{6}$$

Here, A is cross sectional area of the passages for moving gas, ω is working frequency and i is imaginary unit. Re[], Im[] and superscript ~ indicate the real and imaginary parts and conjugation of a complex quantity, respectively. f_k, f_v are thermal and viscous functions. ε_s is the ratio of gas to solid heat capacities. $a,\ c_p,\ k,\ T_m,\ \rho_m, \beta,\ \gamma, \sigma$ are speed of sound, isobaric specific heat capacity, thermal conductivity, mean temperature, mean density, gas expansion coefficient, specific heat ratio and Prandtl number of working gas, respectively.

The numerical solution process of all equations along the x axis is done by employing a fourth-order Runge-Kutta integration method. The calculation of the boundary conditions in DeltaEC uses the shooting method algorithm to solve the integration by initializing a number of "guesses" and meeting the same number of "targets". By setting the "target" boundary conditions somewhere in the model, the "guesses" start to find out their appropriate values that achieve the "targets" and accomplish the convergence of the calculations.

In the current work, DeltaEC modelling tool is applied to obtain the acoustic field including the acoustic power flow in the thermoacoustic generator under consideration. A series of numerical optimizations is performed in order to achieve maximum electrical power output. This includes all axial and lateral dimensions of all components of the generator. Eventually, the optimal configuration is considered for building the experimental set up. For brevity, the results presented in this paper are based on the final optimized configuration.

Figure 2 presents a schematic of the modelled device using DeltaEC segments to construct the representation of the system. An *x*-coordinate is set up for an easy navigation around the system and its subsequent analysis. The origin of the coordinate (x = 0 m) is set at the right end of the cold heat exchanger (CHX) and the positive direction is pointing towards the regenerator (REG) as shown in Figs 2 and 3. Following the *x*-coordinate, the system further contains the hot heat exchanger (HHX) and the thermal buffer tube (TBT). This is followed by the first of two "T-junctions" (x = 0.79 m), a segment referred to as "Resonator" and a second "T-junction" (x = 1.32 m). The main engine loop is then closed by the segment denoted as "Feedback Tube" which meets the beginning of the loop (hence x = 0 m is equivalent to x = 5.04 m). The appropriate equations are integrated from the origin of *x*-coordinate, with pressure values and volumetric velocities matched at the junctions between segments.

The acoustic loop of the generator includes two side branch tubes. These branches are named "Stub1" and "Stub2", and they are located at the two "T-junctions", respectively. The alternator is located at the end of stub 1 while stub 2 contains a sliding piston to change the volume of the tube and match the acoustic impedance between the loop and the alternator. In order to achieve the modelling of one wave length travelling wave system with two branches using DeltaEC, a number of boundary conditions must be defined.

The acoustic pressure amplitude $|p_1|$, the phase of the pressure, ϕ_p, the volumetric velocity amplitude, $|U_1|$, the phase of the volumetric velocity, ϕ_U, and the total power, $\dot{H}$ at the starting point of the loop ($x = 0$ m) must be respectively equal to the same parameters at the "end" of the loop ($x = 5.04$ m):

$$|p_1|_{x\,=\,0\text{ m}} = |p_1|_{x\,=\,5.04\text{ m}}\,, \tag{7}$$

$$(\phi_p)_{x\,=\,0\text{ m}} = (\phi_p)_{x\,=\,5.04\text{m}}\,, \tag{8}$$

$$|U_1|_{x\,=\,0\text{ m}} = |U_1|_{x\,=\,5.04\text{ m}}\,, \tag{9}$$

$$(\phi_U)_{x\,=\,0\text{ m}} = (\phi_U)_{x\,=\,5.04\text{ m}}\,, \tag{10}$$

$$\dot{H}_{2,\ x\,=\,0\text{ m}} = \dot{H}_{2,x\,=\,5.04\text{ m}}\,. \tag{11}$$

At the junction point of the oscillating flow of the first branch (Stub1), the volumetric velocity of the trunk splits into two streams as:

$$(U_1)_{trunk} = (U_1)_{stub1} + (U_1)_{resonator} \,. \tag{12}$$

However, at the split-up point, the pressure amplitude and temperature are the same:

$$|p_1|_{trunk} = |p_1|_{stub1} = |p_1|_{resonator} \,, \tag{13}$$

$$T_{trunk} = T_{stub1} = T_{resonator} \,. \tag{14}$$

The soft end of stub 1 is represented by the acoustic impedance at the back of the alternator being zero:

$$z = \frac{|p_1|}{|U_1|} = 0 \,. \tag{15}$$

Similarly, the conditions for stub 2 are identical to stub 1. However, the hard end is represented by the inverse of acoustic impedance being equal to zero:

$$\frac{1}{z} = \frac{|U_1|}{|p_1|} = 0 \,. \tag{16}$$

The solid temperature of the cold heat exchanger is usually assumed to be fixed at 297 K which matches the average of the cooling water temperature, whereas the solid temperature of the hot heat exchanger is assumed to be fixed at 783 K. When necessary this can also be changed as part of validation against experiments, in particular to account for temperatures measured in two configurations referred to later as with/without housing.

The model of the linear alternator is governed by two boundary conditions. The electric current is guessed to target the load resistance that is connected to the alternator and consumes the produced electric power. Furthermore, the phasing of the electric impedance is targeted at 180 degree by guessing the phasing of the electric current. This step would be done to force the load resistance that is connected to the alternator to be completely resistive in order to extract electric current from the alternator. After setting the boundary conditions according to the above equations and considerations, the process of solving the linear thermoacoustic equations for the whole system was initiated by guessing the solutions that meet the targets, as illustrated earlier.

4. Experimental Apparatus

As discussed above, considering various trade-offs between performance and cost, a looped-tube travelling wave thermoacoustic engine, using atmospheric air as the working gas, is selected from many different engine types and configurations. Furthermore, a standard 8-inch audio loudspeaker (B&C model 8BG51) is introduced as the alternator – the main design factors being its comparatively large transduction efficiency and small value of impedance, following the selection guidelines outlined in [27]. The parameters of the loudspeaker have been measured and are listed in Table 1 against the nominal ones [28]. It should be noted that the measurements were conducted after the unit has been tested in the generator for several hundreds of hours. This is a standard practice in order to "soften" the suspension and obtain a loudspeaker unit of stable mechanical parameters. Consequently, the measured spring factor in Table 1 is much lower than the nominal one, and so is the resonance frequency.

Table 1 Specifications of the loudspeaker (alternator)

	Nominal values	Measured values	Standard Deviation of measured values
F (Hz)	52	40.49	±0.4 %
Bl (N/A)	11.8	11.09	± 0.24%
L_e (mH)	0.5	0.48	±2 %
R_e (Ω)	5.1	5.16	± 0.1%
M_m (g)	35	27.4	± 0.7%
K_m (N/m)	3736	1773	± 1.48%
R_m (kg/s)	0.93	1.23	±1.31 %
X (mm)	+/- 6.5		
A_{alt} (cm2)	220		

The demonstrator has been designed using DeltaEC as described in section 2. It is shown schematically in Fig. 3, while the photograph of the actual unit is shown in Fig. 4. Clearly, the physical device contains the same components as already identified in section 3: a cold heat exchanger (CHX), stacked screen regenerator (REG), hot heat exchanger (HHX), thermal buffer tube (TBT), side branched alternator (ALT), side branched matching stub, and feedback pipe. Figures 3 and 4 also include the information on the associated instrumentation. The total length of the loop is around 5.04 meters, and the operating frequency is around 64 Hz.

Figure 5a shows the construction of the cold heat exchanger. It is manufactured from a block of aluminium. It has the length of 6 cm (in the gas flow direction) and the diameter of 11 cm. 430 openings with the diameter of 3 mm are drilled in the block to provide the channels for the gas flow on the acoustic side of the heat exchanger. Not shown in the photograph, there are 20 openings with 6 mm diameter, drilled perpendicular to the heat exchanger axis in order to provide the passages for cooling water. The porosity of the heat exchanger on the gas side is approximately 0.32.

The regenerator consists of 72 disks "stamped" from a sheet of S/S woven mesh screen. The disks are 11 cm in diameter. The mesh number for the screen used is 34, while the wire diameter is 160 μm. The disks are compressed into the "can" seen on the right of the photograph in Fig. 5b to form a 2.3 cm long regenerator. The calculated porosity of the regenerator is 0.82, while the hydraulic radius is 196 μm. Two thermocouples (type K; TC-Direct model 408-119) are installed at the two regenerator ends (cf. Fig 3.) in order to provide the regenerator temperature difference which is one of the important experimental parameters, as outlined in Section 5.

Figure 5b shows the design of the hot heat exchanger (HHX), which is of shell-and-tube configuration. HHX is made in the form of a "bundle of tubes". Here, 37 S/S tubes with the length of 16 cm, the outer diameter of 1 cm and the wall thickness of 1 mm are welded onto two end plates with holes prefabricated on a triangular matrix with 1.5 cm offset between holes. Subsequently, one end plate is welded to a flanged regenerator "can" while the other to section of tube forming a similarly flanged part of the thermal buffer tube. The resulting porosity of the HHX is approximately 0.196. HHX is heated using a propane gas burner with the heating power which can be adjusted in the range between 0 and 5 kW. The hot gases from the burner flow around the outer surface of the "bundle of tubes". The working gas oscillates inside these tubes which form part of the acoustic network. Three thermocouples are placed inside selected tubes (cf. Fig. 3) to monitor the solid temperature of the tube wall. The configuration of the hot heat exchanger has been chosen as a compromise between the thermoacoustic performance and relative simplicity of manufacture. Welding 37 relatively large diameter tubes (compared to the thermal penetration depth) should be easy to repeat in a "blacksmithing" workshop in remote rural areas as indicated by the socio-economic part of the overall SCORE project.

As indicated above, the section of pipe to the left of the HHX in Fig. 5b forms part of the thermal buffer tube. It has internal diameter of 11 cm, 2 mm wall thickness, and is 17.8 cm long. It also connects to a smaller TBT using a short conical section which reduces the diameter from 11 cm to 5.4 cm over a length of 5.4 cm. The small diameter TBT has a length of 16 cm and internal diameter of 5.4 cm (standard S/S 2-inch pipe, with wall thickness of 2.77 mm). For simplicity, TBT has no thermal insulation and is cooled by the ambient air.

A "T-junction" is connected to TBT (cf. Figs. 3 and 4) through flanges. A branch pipe is connected around 15 cm from the end flange of TBT. It is around 92 cm long, and the alternator is installed at the other end. A second branch pipe (an impedance matching stub) is connected to the resonator through another "T-junction" as already explained in reference [20]. The stub length is much less than a quarter of the wavelength (which is about 5.04 m when the frequency is 64 Hz). The optimized stub length for the configuration discussed here was found to be 480 mm, but this could be changed by the position of the sliding piston as already explained in section 3.

Part of the incident acoustic power is extracted by the branched alternator (enclosed at the back by a compliance volume, illustrated in Figure 4, equipped with a viewing window for the laser displacement sensor), while the remaining acoustic power is transferred back to the cold end of the thermoacoustic core along the feedback pipe, with the total length of 3.77 m. Since in the current design the engine is to be operated with atmospheric air as working gas, the maximum pressure differential between the inside and outside of the rig is that of the acoustic pressure amplitude. As this is typically below 0.15 bar all the low-temperature waveguides could be made of plastic pipes. Therefore, for convenience of construction and reduced costs, the feedback pipe can be made of sections of standard 2-inch PVC pipes and 90° bends (Class E, OD: 60.3 mm, thickness 4.5 mm) instead of metal counterparts.

Five pressure transducers (microphone model 122A22 by PCB PIEZOTRONICS) have been distributed along the rig (cf. locations labelled as P1 through to P5 in Fig. 3) to measure the acoustic pressure amplitudes and relative phase angles. The phase angles between these signals are measured by a lock-in amplifier (model SR830 by DSP) with an accuracy of 0.01º. All of the pressure sensors have a resolution of 7 Pa, and have been calibrated prior to experiments. In addition, a laser displacement sensor (Keyence LK-G152) was installed at the back of the alternator to measure the displacement of the alternator diaphragm. This has a measuring range of ±40 mm with the resolution of 0.5 μm and sampling frequency of 50,000 Hz.

The pressure measurements obtained from P1 and P2 can be used to calculate the acoustic power flow into to the feedback pipe based on a standard two-microphone method [29]. Similarly, the measurements using P3 and P4 can be used to calculate the acoustic power flowing back to the cold end of the thermoacoustic core. The sensor pairs have also been interchanged to double check their reliability. The acoustic power extracted by the loudspeaker (alternator) can be obtained from the pressure measurement in front of the diaphragm using sensor P5 and the diaphragm displacement using the laser displacement sensor. The lock-in amplifier measures the phase angle between these two oscillations and thus a well-established "piston method" is used for calculations [26].

The electrical load for the alternator is simulated by a high power variable resistor. The voltage drop across and the current flowing through the load resistor are measured using a standard laboratory voltmeter (with a resolution of 0.001 V) and ammeter (with a resolution of 0.01 A), thus allowing for estimation of the electrical power as a product of voltage and current.

It needs to be noted that the demonstrator has been tested in two different configurations as far as the combustion process is concerned. They are referred to as "without housing" (or "no housing" in subsequent graphs) and "with housing" (or simply "housing" in subsequent graphs). Figs. 3 and 4 show the "housing" as a metal drum surrounding the propane burner. In the configuration "without housing" the buoyancy drives the flue gas to go around the tube bundle up the chimney, and therefore the air intake and its distribution in the flue gas flow are only controlled by the natural convection processes. The propane flow rate is controlled by a needle valve and, as a result, heating power can be adjusted. However, as the air intake is not controlled, in such experiments, it is not possible to calculate the thermal energy absorbed by the hot heat exchanger.

The configuration "with housing" was introduced in order to carry out some quantitative input power measurements into the hot heat exchanger. In order to estimate the actual heat transfer levels, the flow rate of the flue gas and the temperature drop need to be measured. The air flow needed for the combustion is supplied to the housing through a tube at the bottom. It is regulated by a needle valve and is measured by a rotameter (cf. Fig. 3). Furthermore, two sets of thermocouples were installed in the chimney above and below the hot heat exchanger as shown in Fig. 3, and therefore, the inlet and outlet temperatures of the flue gas could be measured. Combined with the air flow rate, the heat absorbed by the hot heat exchanger could be estimated. This was done assuming a negligible flow rate of propane compared to air.

After the ignition of the propane gas burner, the needle valve in the supply line is opened gradually in several stages to increase the flue gas temperature at the bottom of the HHX. For each step, time of a few minutes was allowed for the temperatures across the HHX and the regenerator to become stable. Accordingly, data for all temperatures, pressure amplitudes and phases, electricity and alternator displacement amplitude and phasing were recorded.

5. Results and Discussion

It is worth noting that in what is to follow, the independent variable is often chosen to be the temperature difference between the hot and cold ends of the regenerator. Of course this choice is arbitrary and alternative approaches are possible. However, this convention is widely accepted in thermoacoustic research (see various papers originating from LANL) and there are a number of reasons for this. Firstly, the temperatures at regenerator ends are directly related to acoustic power gain (see classic papers by Ceperley, e.g. [12]). Secondly, when modelling using DeltaEC such temperatures are easy to target for validation purposes. An alternative choice of the flue gas temperature would be meaningless from the modelling point of view, while another valid choice of heat input being an independent variable would not work for experiments with no housing.

Figure 6 shows measurements of the relationship between the temperature difference between the two ends of the regenerator and the heating temperature of the flue gas at the bottom of the hot heat exchanger. The relationship is almost linear in both cases, with and without housing, the linear trend being slightly better for the latter. It is also seen that the heating temperatures of the flue are higher in the case of housing being present.

In order to verify the modelling results, the collected experimental results of temperatures of the cold and hot sides of the regenerator were targeted in the model for each single measurement and for each case of configuration (i.e. no-housing and housing). This was done by guessing the heat input and heat rejected at the hot and cold heat exchangers. Figures 7 and 8 show the distribution of the acoustic field and power flow along the loop for the cases of no-housing and housing respectively at full power of the burner. They are similar in character but the variables tend to have slightly different magnitudes.

Figure 7a shows the measured and simulated pressure amplitude distribution along the system. The modelling results of the pressure along the loop are shown as a solid line while the measured values are presented as black square symbols. In addition, the white triangles and circles present the acoustic pressure amplitude in the first and second stubs, respectively. There are two maxima and two minima of pressure amplitude along the loop, this behaviour being very similar to already reported characteristics of the same loop equipped with a cooler [30]. The stacked screen regenerator causes a

pressure drop to the oscillating flow. The open end of the branch containing the alternator (Stub1) is a node of the acoustic pressure and the closed end of the tuning stub (Stub2) is an anti-node of the sound pressure. The maximum pressure amplitude at the cold end of the regenerator is around 17 kPa. However, when the burner is enclosed in the housing, the pressure amplitude drops to around 15 kPa as seen in Fig 8a. This indicates that the amount of heat input absorbed by the hot heat exchanger dropped when the housing was installed. Good agreement can be observed in the graph between measured and simulated values for both cases.

Figures 7b and 8b show the modelling results of the distribution of volumetric velocity amplitude along the system for the cases of no-housing and housing, respectively. From both graphs, there are high and low velocity amplitudes along the loop. At the junction of Stub1, the first maximum velocity amplitude is located while the second is located at around 4 m away from the cold side of the regenerator. The two smallest velocity amplitudes are located at (x= 0 m) and (x= 2.6 m) in the loop. From both graphs it can also be noticed that the temperature gradient in the regenerator causes a steep increase in the velocity while the two stubs cause a sharp fall. It can also be seen that the ends of Stub1 and Stub2, are a velocity anti-node and velocity node, respectively. From the graphs, the alternator is located at high velocity amplitude in Stub1. This is one of the design targets to achieve high velocity amplitude that is capable to drive the alternator to maximum displacement. In Fig 7b, the maximum velocity amplitude achieved at the hot side of the regenerator is around 0.045 m^3/s. However, when the housing is included the velocity amplitude falls to around 0.04 m^3/s as shown in Fig 8b.

Figures 7c and 8c present the acoustic impedance distribution in the generator for the case of no-housing and housing, respectively. From both figures, there are two maxima and minima along the loop. The two maximum points are located at the cold side of the regenerator and around 2.5 m away from the regenerator. The two minimum acoustic impedance points are located at 1.2 and 3.8 m away from the regenerator. The significant fall of the acoustic impedance in the regenerator is attributed to the fall of the pressure amplitude and the increase of the velocity amplitude. Moreover, the introduction of Stub1 and Stub2 in the loop, slightly increases the acoustic impedance. This is due to the volumetric velocity flows into the stubs as seen in Figs 7b and 8b.

Figures 7d and 8d show the acoustic impedance phasing along the loop for the two cases. From the graph, the regenerator is located in the region of ($-23.71° < \phi < -7.38°$) while the phase difference between the pressure and velocity along the loop ranges between around 60^o and -60^o. Figures 7e and 8e show the measured and calculated acoustic power flow along the system for the no-housing and housing configurations. As seen in Fig 7e, around 221 W of acoustic power enters the ambient heat

exchanger and 218 W passes into the ambient end of the regenerator. The regenerator amplifies the 218 W to around 345 W that is fed into the hot heat exchanger. Around 35 W and 29 W of acoustic power is lost in the hot heat exchanger and thermal buffer tube, respectively. Stub1 receives 35 W and 32.4 W is extracted by the alternator. The modelling results show that at 10 Ω of load resistance and 479 W of heat input, the electrical power output is 18.4 W. This gives thermal-to-acoustic efficiency of around 6.8%, thermal-to-electric efficiency of 3.87% and alternator efficiency of 56.914%. However, when the housing is introduced, the acoustic power drops from 345 to 266 W at the hot end of the regenerator as seen in Fig 8e. Here the modelling results show electrical power around 14.5 W and heating power around 387 W. This yields thermal-to-electric efficiency of 3.73% and thermal-to-acoustic efficiency of 6.565%.

Figure 9 shows a comparison between the simulation and the measurements related to the effect of the temperature difference between the two sides of the regenerator on the coil displacement of the alternator. The measured results are shown as white circles and black triangles, while DeltaEC results are presented as a solid line and dash line in the cases of no-housing and housing, respectively. The calculations and measurements have a similar trend of almost a linear increase of the coil displacement within the increase of the temperature difference. In the case of no-housing, the increase of the temperature difference from 240 K to 340 K causes a gradual rise in the measured coil displacement from around 2.81 mm to around 6.88 mm and calculated increase from 4.55 to 6.44 mm. However, the results of coil displacement are significantly affected by containing the burner in the housing. The measured displacement raises from 2.67 to 6.1 mm whereas the calculated displacement goes up from 3.74 to 5.72 mm when the temperature difference is increased from 236.5 to 337.5 K. It is clear from the graph that there is a good agreement between the simulated and experimental results especially at high temperature differences.

Figure 10 shows a comparison between the calculated and measured effects of the temperature difference of the regenerator on the acoustic power that is extracted by the alternator in the cases of "with" and "without" the housing. The graph clearly shows that both the calculated and measured results of the acoustic power extraction have an almost linear relationship with the temperature difference. When there is no housing in the experimental setup, the increase in the temperature difference increases the measured extraction of the acoustic power from 5.04 W to the maximum value of around 37.18 W and increases the calculated acoustic power from 15.9 to 32.34 W. However when the housing is introduced to the setup, both measured and calculated results drop considerably particularly at high temperature differences. In this case the maximum measured and calculated acoustic powers are 26.44 and 25.44 W, respectively.

Figure 11 shows the relationship between the temperature difference of the regenerator and the electrical output of the generator. The relationship is presented as a comparison between the calculated and measured results for the two cases of burner configurations. The graph indicates that as the temperature difference increases so does the electrical output. The maximum measured and simulated electrical power values are 17.8 and 18.4 W, respectively (for no-housing configuration). The corresponding values fall to 14.14 and 14.16 W when the burner is enclosed in the housing. Generally speaking, the measured and the simulated results are in a good agreement at the range of temperature difference from 280 to 340 K.

The variation of results between cases "with" and "without" housing, as shown in Figs. 9, 10 and 11, can be explained by the difference in the heat input for each configuration as seen in Fig 12. This can be attributed to the fact that the flow rate of the compressed air supplied to the housing for combustion is much smaller than that supplied by natural convection in the case of no-housing. This inference can also be drawn from Fig. 6 as the flue gas temperature at the bottom of the chimney in the case of the housing is higher than that for no-housing. Indeed, the temperature difference of the rising flue gas across the hot heat exchanger is higher in the case of housing as seen in Fig 13. An additional factor may be that the compressed air flow in the housing may not be uniformly distributed over the housing. This would affect both the heat transfer rates and the horizontal temperature distribution of the hot heat exchanger.

It can be observed in Fig. 12 that, when plotting the simulated heat input versus the temperature difference along the regenerator, the case with "no housing" has heat input values consistently higher (by about 70-90 W) than the case with the housing in place, which is consistent with the discussion above. However, one can also see in Fig 12 that for the case of the housing, the experimental heat input is much higher than for any of the simulated ones. This is due to the fact that substantial amount of the measured heat input is lost by conduction in HHX tubes, the S/S enclosure as well as a portion of the heat being possibly dissipated to the surroundings. These aspects cannot be taken into account in DeltaEC simulations.

Following the data presented in Figs 10 and 12, the efficiency of the thermoacoustic engine can be evaluated. Figure 14 presents the influence of the temperature difference of the regenerator on the thermal-to-acoustic efficiency of the electricity generator. The graph shows a comparison between the measured and calculated results, for the case of the housing present, in black triangles and a dashed line, respectively, as well as the simulated results for the no-housing case in a solid line. It is shown that the efficiencies increase in an almost linear manner as the temperature difference is increased. In addition, the modelled efficiency in the case of no-housing is in percentage terms around 3% higher

than that in the case of housing when the temperature difference reaches 340 K. Furthermore, the measured thermal-to-acoustic efficiency increases from 2 to 3.5% when the temperature difference of the regenerator increases from 260 to 340 K.

Similary, based on the results shown in Figs.11 and 12, the thermal-to-electric conversion efficiency can be evaluated as shown in Fig.15. The majority of the measured cases have a thermal-to-electric efficieny in a range 1.5-2% for a range of the temperature difference between 280 and 340 K. However, the simulated effeciencies are much higher for the reasons discussed above and at high temperature difference, they can reach 3.7 and 3.85% for housing and no-housing configurations, repectively.

Figure 16 shows the comparison between measured and simulated results of the alternator efficiency (i.e. acoustic-to-electric efficiency) as a function of the regenerator temperature difference. It is seen from the graph that both measured and calculated results fall onto a relatively flat horizontal line when plotting their dependence on the temperature difference. The acoustic-to-electric efficiency of the alternator is usually considerably affected by the electric load resistance [20]. However, because the load resistance is fixed at 10 Ω for the purpose of modelling, there is no effect on the alternator efficiency and simulation results have simply a fixed value of 56.914%. The measured efficiencies for both experimental cases drop from around 63% to around 45% along the increase of the temperature difference. The displacment of the diphragm of the alternator increases as the power output increases. Hence the coil begins to come out from the magnet gap until it finally reaches its maximum displacemnt at temperature difference higher than 320^{o}C, as also seen in Fig 9. This feature is not considered in the simulations where there is no limitation on the alternator displacement and the effect of the coil coming out of the magnet gap cannot be predicted.

Similar effects are included in Fig 17 which shows the relationship between the coil displacement and the acoustic-to-electric efficiency. It can be observed that the efficiency drops below 50% when the displacement exceeds 6.5 mm in the case of no-housing. Figure 18 shows the effect of the electrical load on the electrical output of the alternator in both simulation and experiments at full power of the burner. Here, the electricity is also proportional to the load resistance when the load is raised from 5 to 10 Ω. As a result, the electric power extracted from the alternator increases from 15.2 to around 17.8 W. However, when the load was further increased to 19 Ω, the electrical power dropped slightly to 15.5 W. So it is clear that a resistance of around 10 Ω is the optimum load that extracts the maximum electric power from the alternator.

6. Conclusions and future work

This paper presents the design, modelling, construction and testing of a travelling wave thermoacoustic electricity generator that converts thermal power to electricity using a "side-branched" audio loudspeaker. For the purpose of demonstration, flue gas at temperature over 500°C provided by propane combustion is utilized to supply thermal energy to the hot heat exchanger of the thermoacoustic generator. The experimental results show that the generator can produce up to 17.8 W of electrical power with thermal-to-acoustic efficiency of 3.5% and thermal-to-electric efficiency of up to about 1.9%. The demonstrator presented in this paper shows the viability of a micro-electricity generator based on thermoacoustic technology that can be driven by waste heat from the cooking activities typical for remote and rural areas of developing countries.

For the optimized configuration, it is shown that that there is a good agreement between the measurements and the simulations based on DeltaEC modelling tool especially for the temperature differences between the two ends of the regenerator in the high range of the temperature conditions investigated. However, substantial disagreement between calculations and measurements can be found at low temperature differences. There are a number of further steps that need to be taken in order to deliver a higher electrical output power (broadly in a range 50-150 W). This can be achieved using a number of approaches including (i) geometrical scale-up of the device, (ii) improvements in the design of the heat exchangers – in particular HHX, (iii) selection of loudspeakers with more favourable characteristics and/or their in house modifications, (iv) considering multiple-stage thermoacoustic engines to better utilize the thermoacoustic energy conversion mechanisms.

Finally, it is worth pointing out that in order to adopt the technology in future one would need to look into suitable electronics to rectify the obtained output and make it suitable for battery charging. Similarly, suitable variants of the device may be developed to utilize solar energy as an input.

Acknowledgments

Kalid Abdoulla-Latiwish would like to express his thanks to the Libyan government for funding his PhD studies under supervision of Prof. Jaworski and Dr Mao. Artur J. Jaworski would like to acknowledge funding received from EPSRC (grant EP/E044379) and the Royal Society Industry Fellowship (grant IF110094). Dr H. Kang of Beijing Institute of Technology is acknowledged for her help in training Dr Abdoulla-Latiwish in the use of DeltaEC modelling software during her secondment as a visiting academic in Prof. Jaworski's thermoacoustics group. Dr Z. Yu – formerly a PDRA in Prof. Jaworski's thermoacoustics group – is gratefully acknowledged for collecting the experimental data for the project. Other partners in the overall SCORE project: University of

Nottingham, City University London, Queen Mary University of London and Practical Action are acknowledged for useful collaborations within the SCORE project.

References

[1] J. W. Strutt (Lord Rayleigh), The Theory of Sound, 2nd ed., Dover Publications, New York, 1894, vol. 2, sec. 322

[2] G. W. Swift. Analysis and performance of a large thermoacoustic engine. J. Acoust. Soc. Am. 1992; 92 (3): 1551-1563

[3] J. R. Olson and G. W. Swift. A loaded thermoacoustic engine. J. Acoust. Soc. Am. 1995; 98 (5): 2690-2693

[4] J. J. Wollan, G. W. Swift, S. Backhaus and D. L. Gardner, "Development of a thermoacoustic natural gas liquefier," Proceedings of AIChE Meeting, New Orleans LA, March 11-14, 2002; see also http://lib-www.lanl.gov/la-pubs/00796080.pdf.

[5] S. Backhaus and G. W. Swift. A thermoacoustic-Stirling heat engine: Detailed study. J. Acoust. Soc. Am. 2000; 107:3148-3166.

[6] H. Sugita, Y. Matsubar, A. Kushino, T. Ohnishi, H. Kobayashi and W. Dai. Experimental study on thermally actuated pressure wave generator for space cryocooler. Cryogenics. 2004; 44: 431–437.

[7] D. L. Gardner and G. W. Swift. A cascade thermoacoustic engine. J. Acoust. Soc. Am. 2003; 114 (4), 1906-1919.

[8] T. Yazaki, A. Iwata, T. Maekawa and A. Tominaga. Traveling wave thermoacoustic engine in a looped tube. Phys. Rev. Lett. 1998; 81: 3128–3131.

[9] C. M. de Blok. Low Operating Temperature Integral Thermoacoustic Devices for Solar Cooling and Waste Heat Recovery. Acoustics'08 2008, June 29-July 4. Paris, France

[10] Z. Yu and A. J. Jaworski. Impact of acoustic impedance and flow resistance on the power output capacity of the regenerators in travelling-wave thermoacoustic engines. Energy Conversion and Management 2010, 51: 350–359

[11] P. H. Ceperley. A pistonless Stirling engine–The traveling wave heat engine. J. Acoust. Soc. Am., 1979; 66: 1508-1513.

[12] P. H. Ceperley. Gain and efficiency of a short traveling wave heat engine. J. Acoust. Soc. Am., 1985; 77: 1239-1244.

[13] M. E. H. Tijani and S. Spoelstra. A high performance thermoacoustic engine. J. Appl. Phys. 110, 093519 (2011)

[14] S. Backhaus, E. Tward and M. Petach. Travelling-wave thermoacoustic electric generator. Appl Phys Lett 2004; 85(6): 1085–1087.

[15] Z. H. Wu, M. Man, E. C. Luo, et al. Experimental investigation of a 500 W traveling-wave thermoacoustic electricity generator. Chinese Sci Bull, 2011, 56:1975-1977

[16] T. Sanchez, H. Owala and V. Okello. Research into the Behaviour of Rural Families to Technology Changes, Proc. Of International Conference on "Low-cost, electricity generating heat engines for rural areas, 2-3 April 2012, Nottingham, UK

[17] T Sanchez, R. Dennis and K. Pullen. Cooking and lighting habits in rural Nepal and Uganda – SCORE Project, Proc. Of International Conference on "Low-cost, electricity generating heat engines for rural areas, 2-3 April 2012, Nottingham, UK

[18] R. Dennis and K. Pullen. Development of wood-fired cooking stove to incorporate a thermo-acoustic engine-generator unit, Proc. Of International Conference on "Low-cost, electricity generating heat engines for rural areas, 2-3 April 2012, Nottingham, UK

[19] P. Saechan, Z. Yu and A. J. Jaworski. Design and experimental evaluation of a travelling wave thermoacoustic cooler driven by a standing wave thermoacoustic engine, Proc. 19th International Congress on Sound and Vibration, 2012, 8-12 July, Vilnius, Lithuania

[20] Z. Yu, A. J. Jaworski and S. Backhaus. Travelling-wave thermoacoustic electricity generator using an ultra-compliant alternator for utilization of low-grade thermal energy. Applied Energy 2012; 99: 135-145

[21] Swift G W. Thermoacoustic engine. J. Acoust. Soc. Am. 1988; 84(4): 1145-1180.

[22] H. Kang, P. Cheng, Z. Yu and H. Zheng. A two-stage traveling-wave thermoacoustic electric generator with loudspeakers as alternators. Applied Energy. 2015; 137:9-17.

[23] M. E. Tijani, J. C. Zeegers and A. T. De Waele. Design of thermoacoustic refrigerators. Cryogenics. 2002; 42(1):49-57.

[24] W. C. Ward and G. W. Swift. Design environment for low-amplitude thermoacoustic engines. J. Acoust. Soc. Am. 1994; 95: 3671–3672.

[25] B. Ward, J. Clark and G. W. Swift. Design Environment for Low Amplitude Thermoacoustic Energy Conversion DeltaEC Version 6.3 b11 Users Guide. Los Alamos national laboratory. 2012.

[26] G. W. Swift. Thermoacoustics: A Unifying Perspective for some Engines and Refrigerators. New York, Acoustical Society of America, 2002.

[27] Z. Yu, P. Saechan and A. J. Jaworski. A method of characterising performance of audio loudspeakers for linear alternator applications in low-cost thermoacoustic electricity generators. Applied acoustics. 2011; 72(5):260-7.

[28] http://www.bcspeakers.com/

[29] A. M. Fusco, W. C. Ward and G. W. Swift. Two-sensor power measurements in lossy ducts. J. Acoust. Soc. Am. 1992: 91(4): 2229-2235.

[30] P. Saechan, H. F. Kang, X. Mao and A. J. Jaworski. Thermoacoustic refrigerator driven by a combustion-powered thermoacoustic engine – demonstrator of device for rural areas of developing countries, *Proc. World Congress on Engineering*, Vol. III, 2097-2102, London, UK, 3-5 July 2013

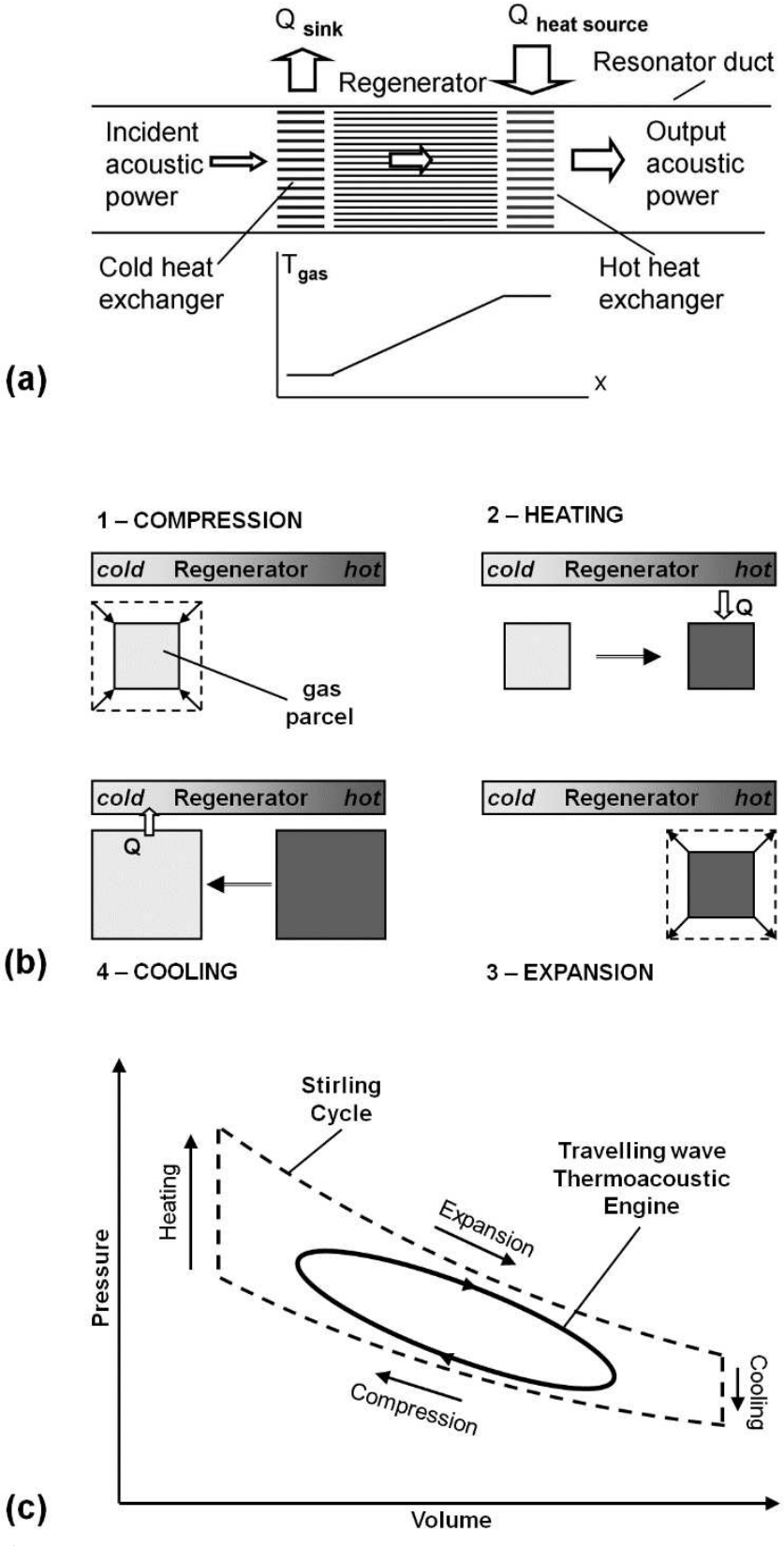

Fig. 1 Explanation of the thermodynamic processes behind operation of travelling wave thermoacoustic engine: (a) schematic of the engine "core"; (b) schematic of the gas parcel state and heat transfer interactions; (c) thermoacoustic Stirling-like cycle vs. classical Stirling cycle

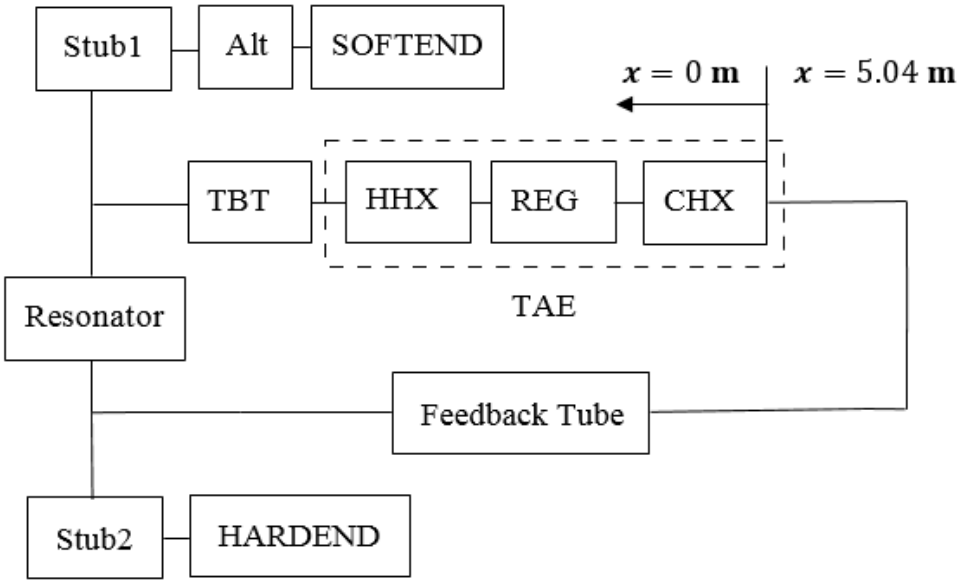

Fig. 2 Diagram of the DeltaEC segments including: ambient heat exchanger (AHX), regenerator (REG), hot heat exchanger (HHX), thermal buffer tube (TBT), the first stub where the alternator is located at the end (Stub1), the linear alternator (Alt), the tube between the first stub and the second stub (resonator), the feedback tube and the second stub with adjustable piston (Stub2 + HARDEND).

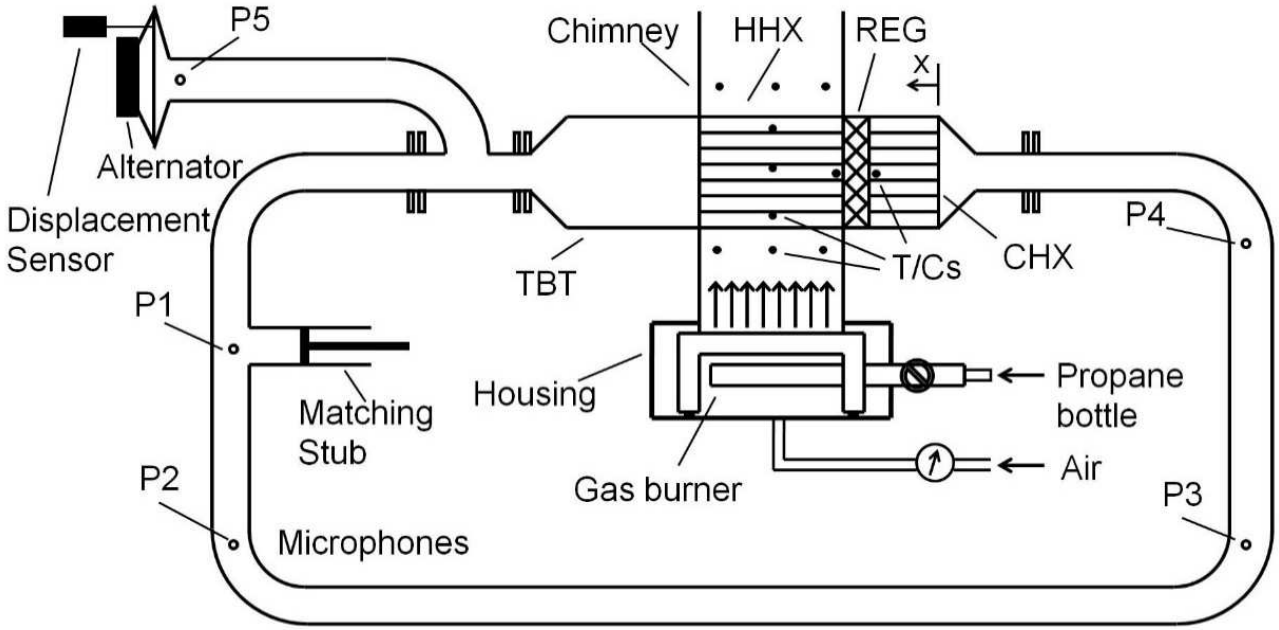

Fig. 3 Schematic illustration of the tested thermoacoustic generator

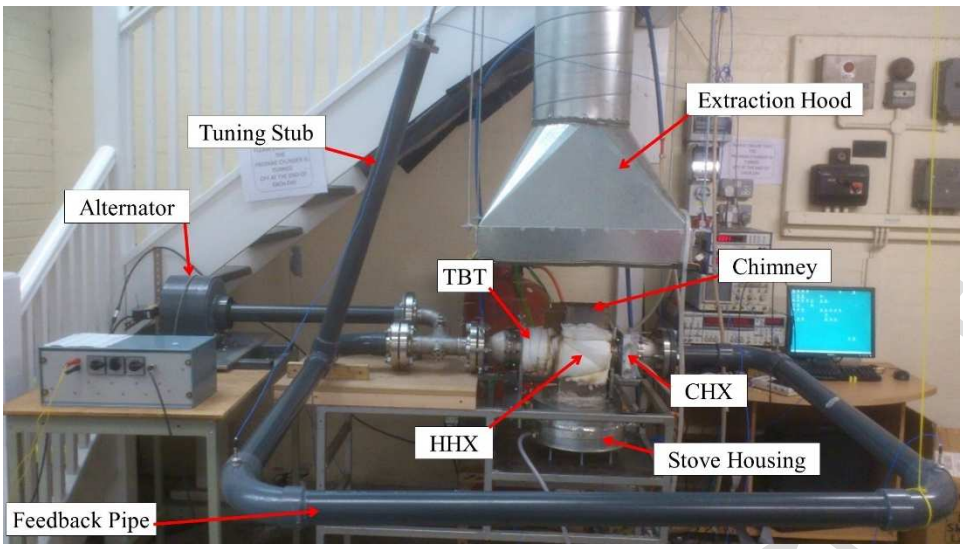

Fig. 4 Photograph of the tested thermoacoustic generator

(a) *(b)*

Fig. 5 Photographs of (a) the cold heat exchanger (CHX) and (b) the hot heat exchanger (HHX)

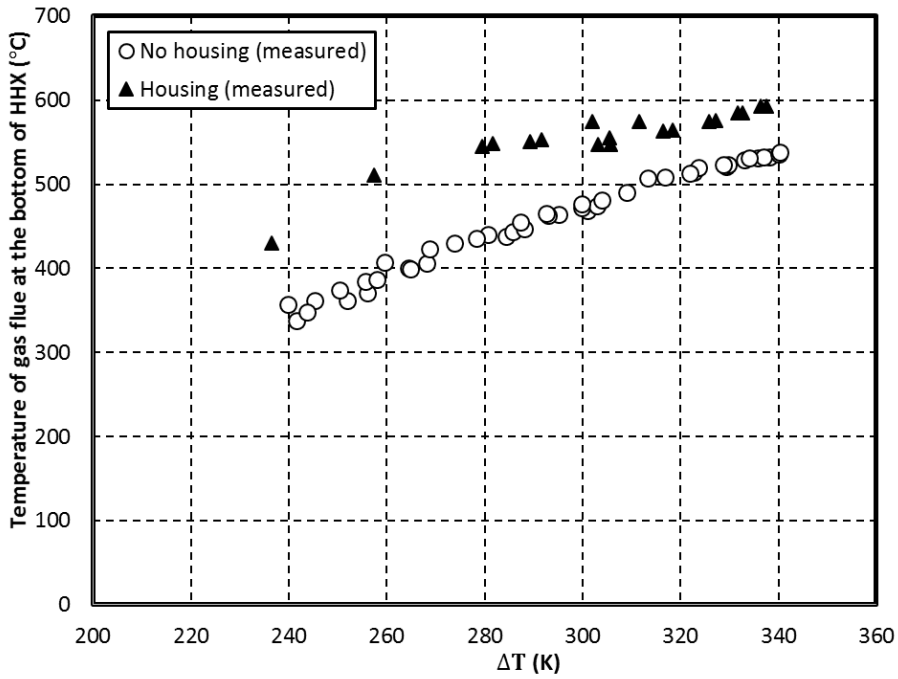

Fig. 6 The gas flue heating temperature at the bottom of the HHX versus the temperature difference between two ends of the regenerator

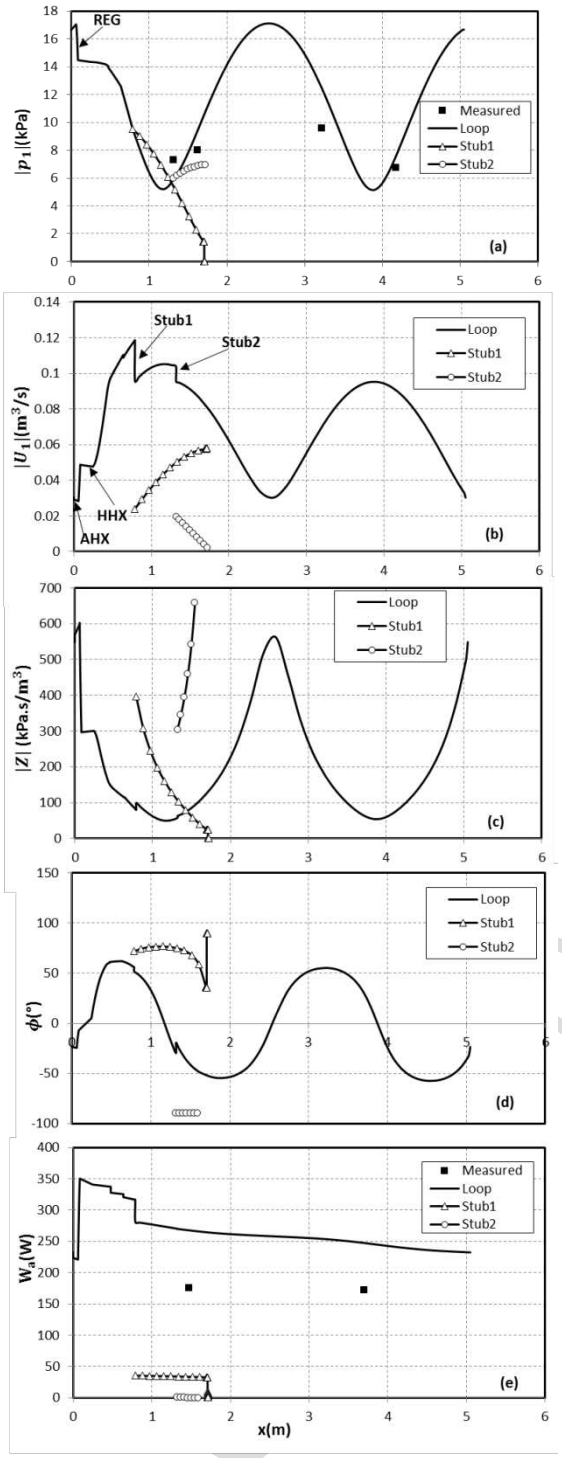

Fig. 7 The distributions of the acoustic power flow and the acoustic field in the electricity generator in the case of no-housing. (a) Pressure amplitude, (b) Volumetric velocity, (c) Acoustic impedance (d) Phase angle and (e) Acoustic power flow.

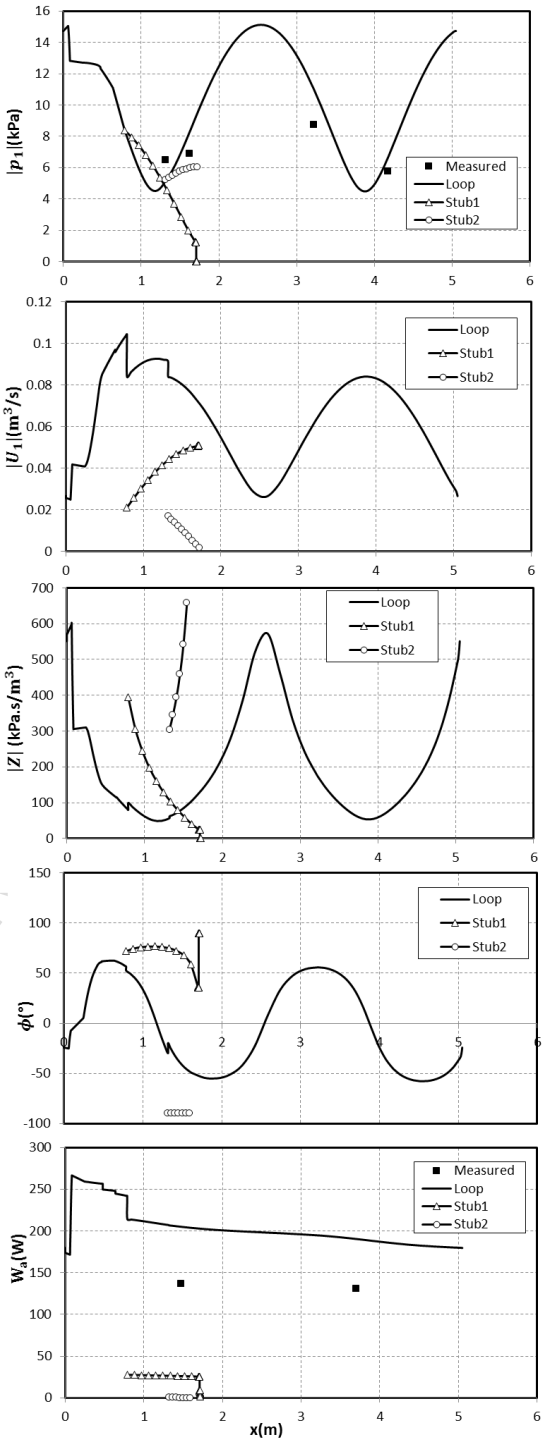

Fig. 8 The distributions of the acoustic power flow and the acoustic field in the electricity generator in the case of housing. (a) Pressure amplitude, (b) Volumetric velocity, (c) Acoustic impedance (d) Phase angle and (e) Acoustic power flow.

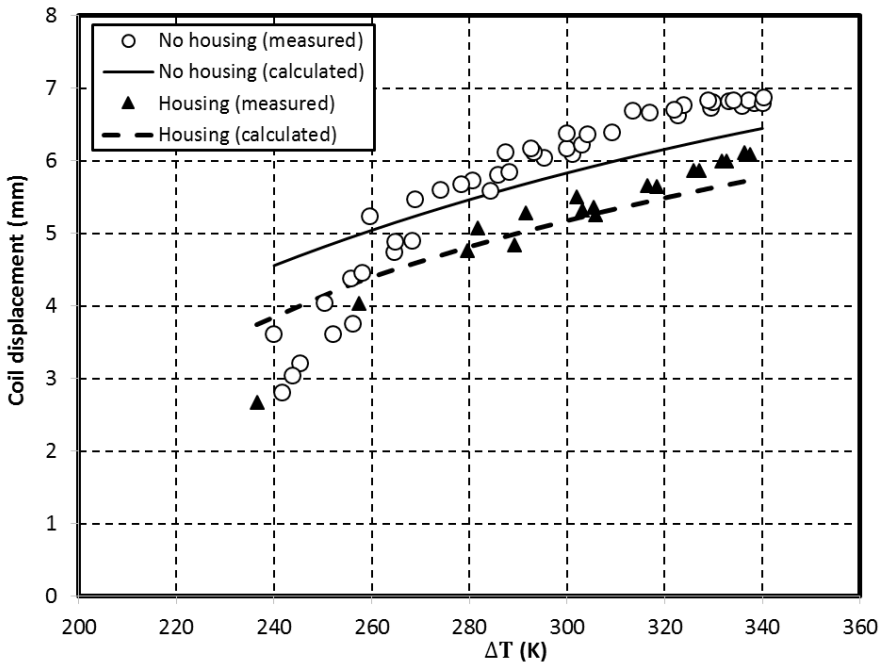

Fig. 9 The effect of the temperature difference between the two ends of the regenerator on the coil displacement of the alternator

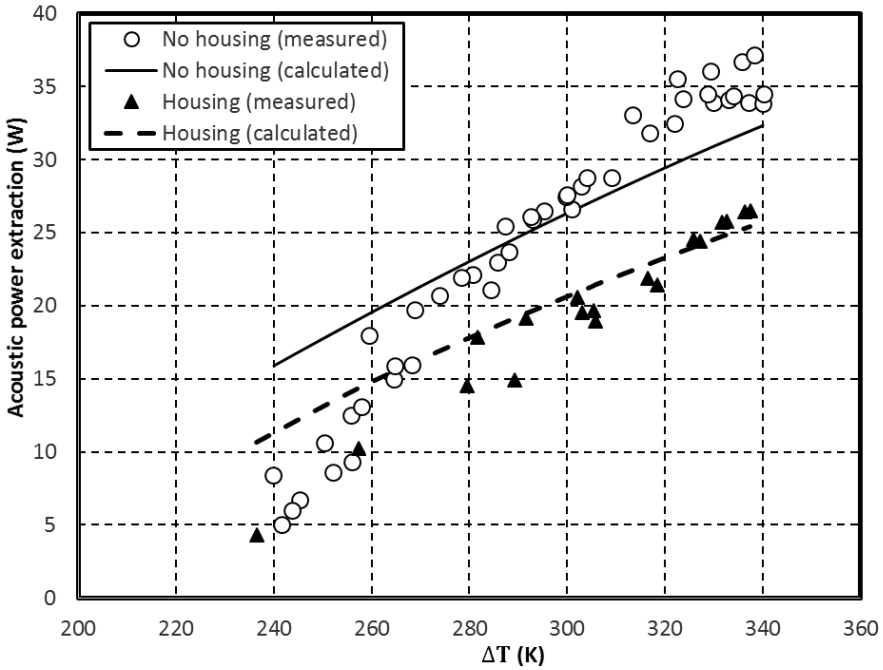

Fig. 10 The effect of the temperature difference between the two ends of the regenerator on the acoustic power extraction of the alternator

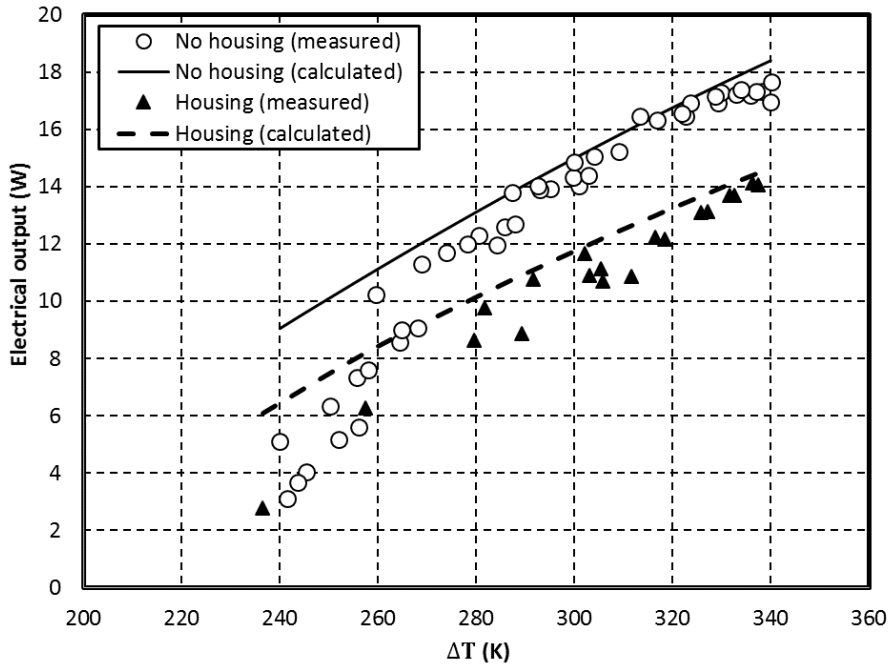

Fig. 11 The effect of the temperature difference between the two ends of the regenerator on the electrical output of the alternator

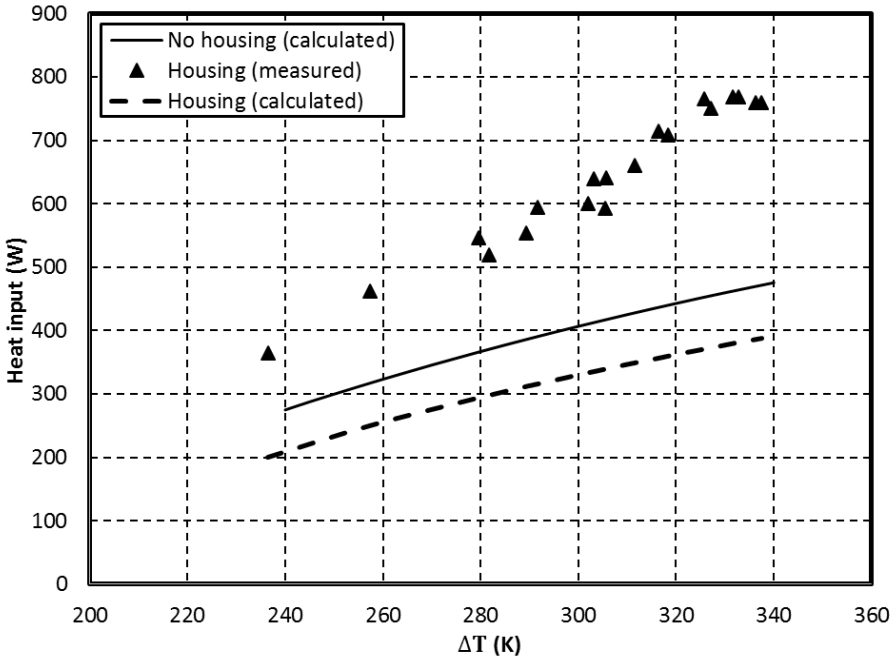

Fig.12 Measured and simulated relationships between heating power and the temperature difference between two ends of the regenerator

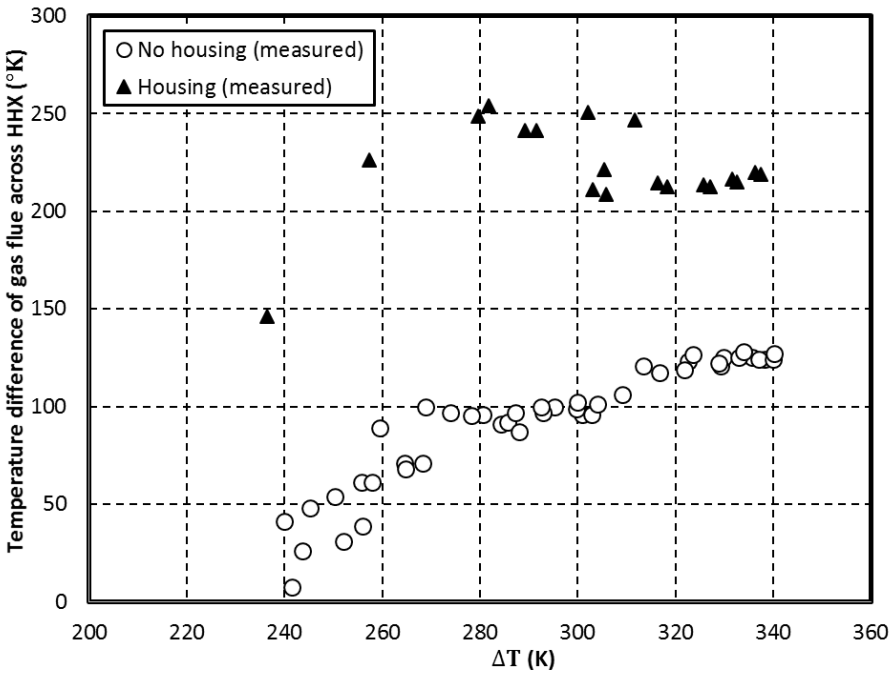

Fig.13 The gas flue temperature difference across the HHX versus the temperature difference between two ends of the regenerator

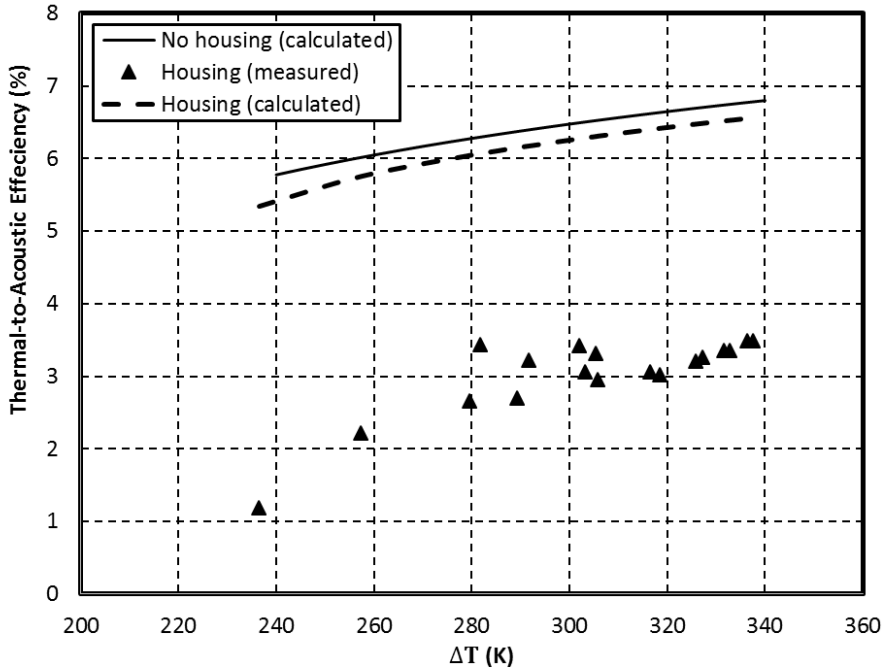

Fig.14 The effect of the temperature difference between the two ends of the regenerator on the thermal-to-acoustic efficiency

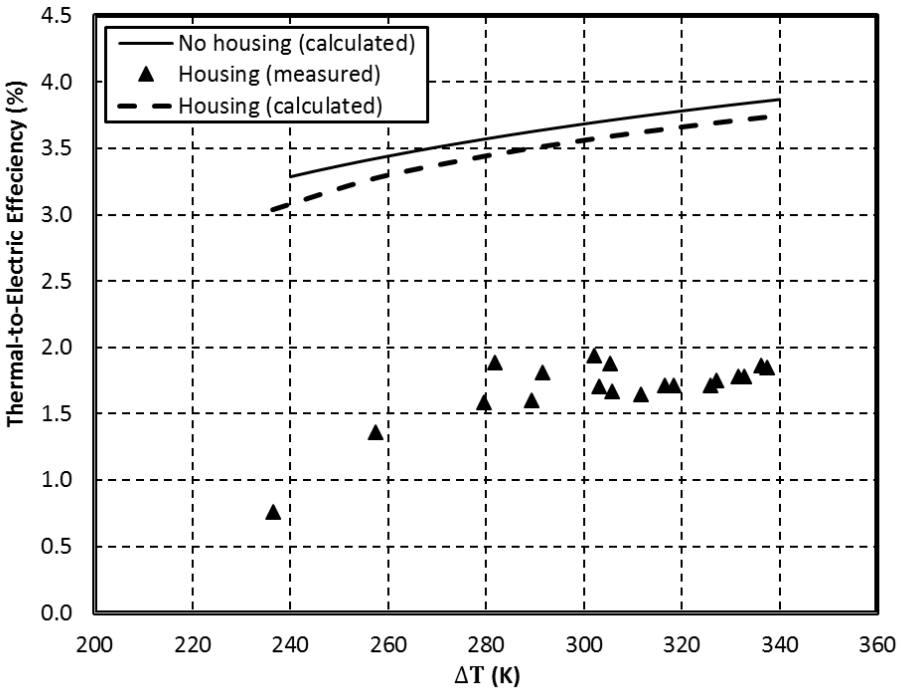

Fig.15 The effect of the temperature difference between the two ends of the regenerator on the thermal-to-electrical efficiency

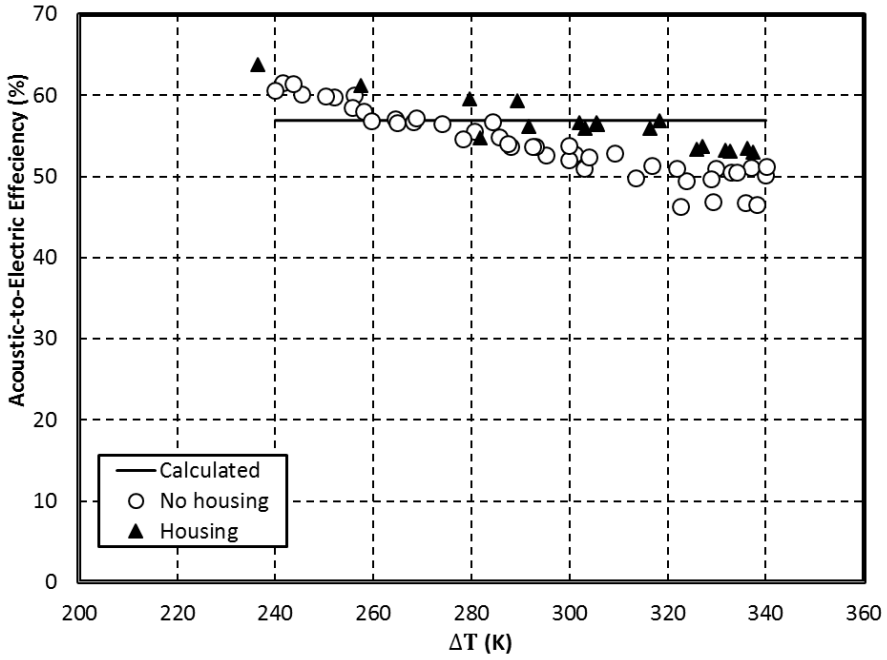

Fig.16 The effect of the temperature difference between the two ends of the regenerator on the alternator efficiency

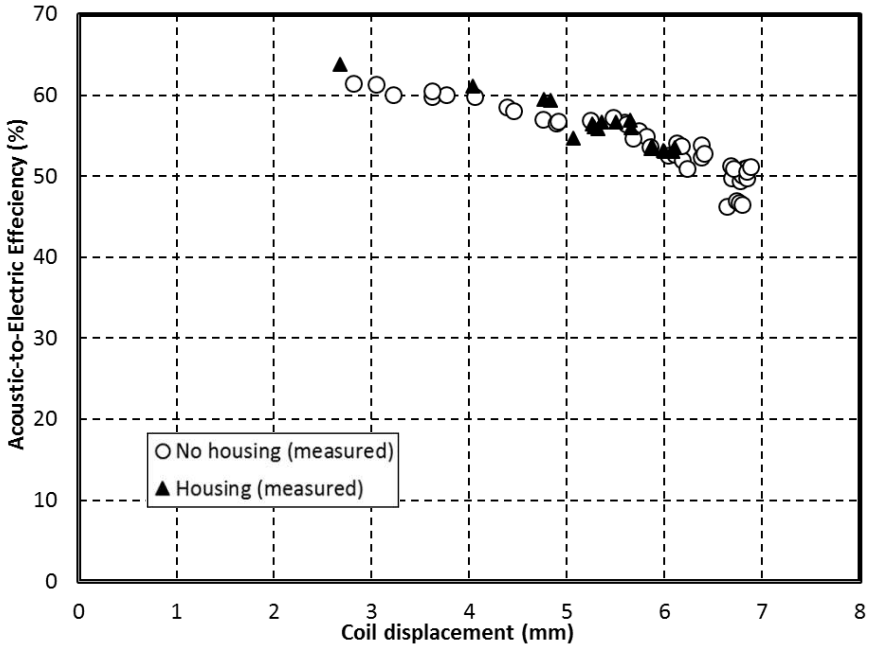

Fig.17 The dependence of the acoustic-to-electric efficiency on the coil displacement amplitudes

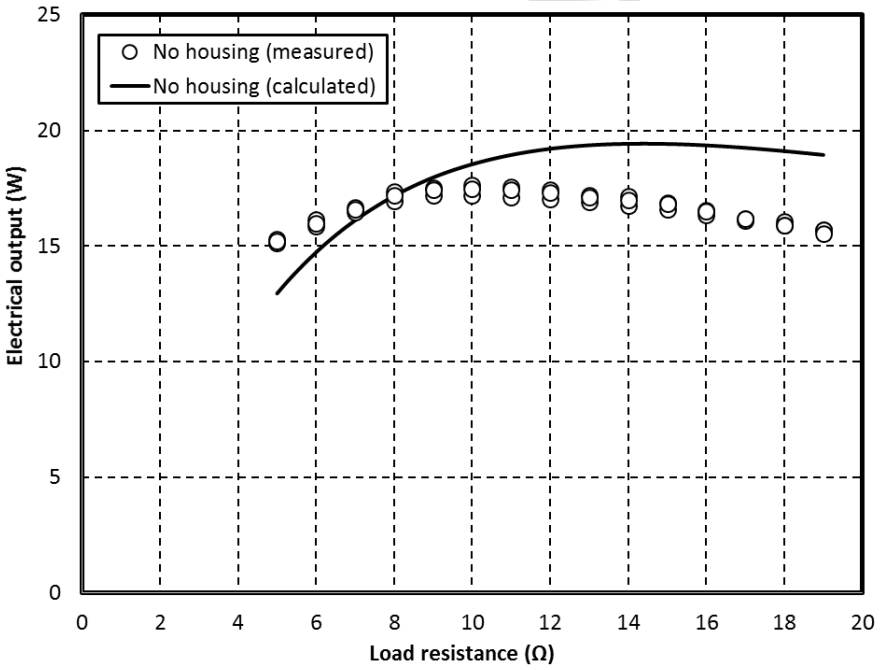

Fig.18 The measured relationship between electric power output and the load resistance of the alternator when the gas burner operates at full power level (ΔT = 340K)